Authors' response to review of "Northern high-latitude permafrost and terrestrial carbon response to solar geoengineering" by Chen et al.

We thank your constructive comments, which help us clarify and greatly improve the study. In the following, comments from the referee are in black, our responses are in blue.

General comment

The authors studied how the permafrost extent and terrestrial carbon fluxes and pools are in response to two solar geoengineering scenarios, ssp245 and 585 scenarios based on CMIP6 simulations. The topic is timely and fits the scope of the journal Earth System Dynamics. The paper is well structured and the results are well illustrated in the figures. However, the authors need to put more effort to explain how the difference in surface climate between solar geoengineering scenarios and ssp245 affects soil surface temperature, NPP, and ER. Vegetation response to climate forcing plays a major role here. It is strange that G6solar and G6sulfur have lower radiation or summer temperature than ssp245, but they still have higher NPP and ER. Also, snow duration and surface litter are important insulators for soil freezing and thawing. I suggest the authors should mention these aspects in their discussion. Finally, the authors should polish the language further and avoid some grammar mistakes.

Thank you for your constructive comments. We would like to respond to your questions in the general comment as follows:

1. The authors need to put more effort to explain how the difference in surface climate between solar geoengineering scenarios and ssp245 affects soil surface temperature, NPP, and ER. Vegetation response to climate forcing plays a major role here.

Thanks for your suggestions. A very robust finding of solar geoengineering under GeoMIP scenarios with equatorial stratospheric injections is high-latitude residual warming (Kravitz et al., 2013a; Yu et al., 2015; Muri et al., 2018; Russotto and Ackerman, 2018; Henry and Merlis, 2020; Visioni et al., 2021). High latitude near-surface air temperatures are generally higher under G6solar and G6sulfur than ssp245, especially over northern Eurasia (Visioni et al., 2021). The impacts of differences in surface climate on soil surface temperature depends on the thermal insulation of snow and litter layers. The five earth system models (ESMs) used in this study all adopt multi-layered snow schemes and consider the thermal effects of soil organic matter, but no explicit litter layer. The largest differences between near-surface air temperature and soil surface temperature occur in winter, when the snow pack creates strong thermal insulation. In the $PF_{50\%}$ region, the differences in snow coverage and snow depth are statistically insignificant between G6solar and ssp245, while the snow depth under G6sulfur is slightly thicker than ssp245 due to more snowfall in winter (Figure R1r). However, the averaged thermal offset (measured as soil temperature at 0.2 m depth minus near-surface air temperature) over the $PF_{50\%}$ region during the period 2080-2099 are 4.0±2.4, 3.9±2.3 and 4.1±2.4 ºC for G6solar, G6sulfur and ssp245 respectively, their differences are considerably smaller than the magnitude of residual warming in near-surface air. The spatial patterns of residual warming in near-surface air and 0.2 m depth soil are similar (Figure R1e vs R1i, R1f vs R1j, R1g vs R1k, R1h vs R1l). In winter, the magnitude of residual warming in soil at 0.2 m depth (Figure R1i-j) is relatively smaller than near-surface air (Figure R1e-f) mostly due to thermal insulation of snow layers, and the residual warming attenuates further at 2 m depth soil (Figure R1m-n). In summer, the residual warming in near-surface air (Figure R1g-h) is less pronounced in both G6solar

and G6sulfur than winter. However, the residual warming in soil at 2 m depth (Figure R1p) is more pronounced than near-surface air (Figure R1h) under G6sulfur. This is due to the profound residual winter warming in near-surface air affecting the summer soil at deep layers (Burn and Zhang, 2010) as discussed in the manuscript L194-200. This also occurs under G6solar as evidenced by the residual summer warming in soil at 2m depth (Figure R1o) being slightly larger the residual winter warming (Figure R1m).

The differences in NPP mirror more directly structural and parametric differences in land surface models, in particular the carbon assimilation scheme that depends on nutrient limitation. The models which represent land nitrogen cycle (CESM2-WACCM, MPI-ESM1-2-LR and UKESM1-0-LL) simulate similar NPP magnitudes (~ 3 Pg C yr^{-1}) during baseline period (1995-2014). Except for CNRM-ESM2-1, NPP increases in the other four models under G6solar/G6sulfur and ssp245 are similar (Figure R2), consistent with their comparable land carbon-concentration feedback parameters (Table A1 in Arora et al., 2020). CNRM-ESM2-1 has similar NPP increases under G6solar/G6sulfur and ssp585 (Figure R2c), probably due to its land carbon-concentration feedback parameter is largest in the five models (Table A1 in Arora et al., 2020). In addition to the differences in land surface models, part of the inter-model spread of NPP response comes from the ESMs' response to future climate scenarios. To disentangle the relative magnitude of uncertainties contributed from the ESMs' response to future climate scenarios, we added a group of experiments by using the anomaly forcing CLM5 method, please see our reply to your 14th specific comment.

Our further response to the question on "how the difference in surface climate between solar geoengineering scenarios and ssp245 affects NPP and ER", is addressed in our reply to your 12th specific comment.

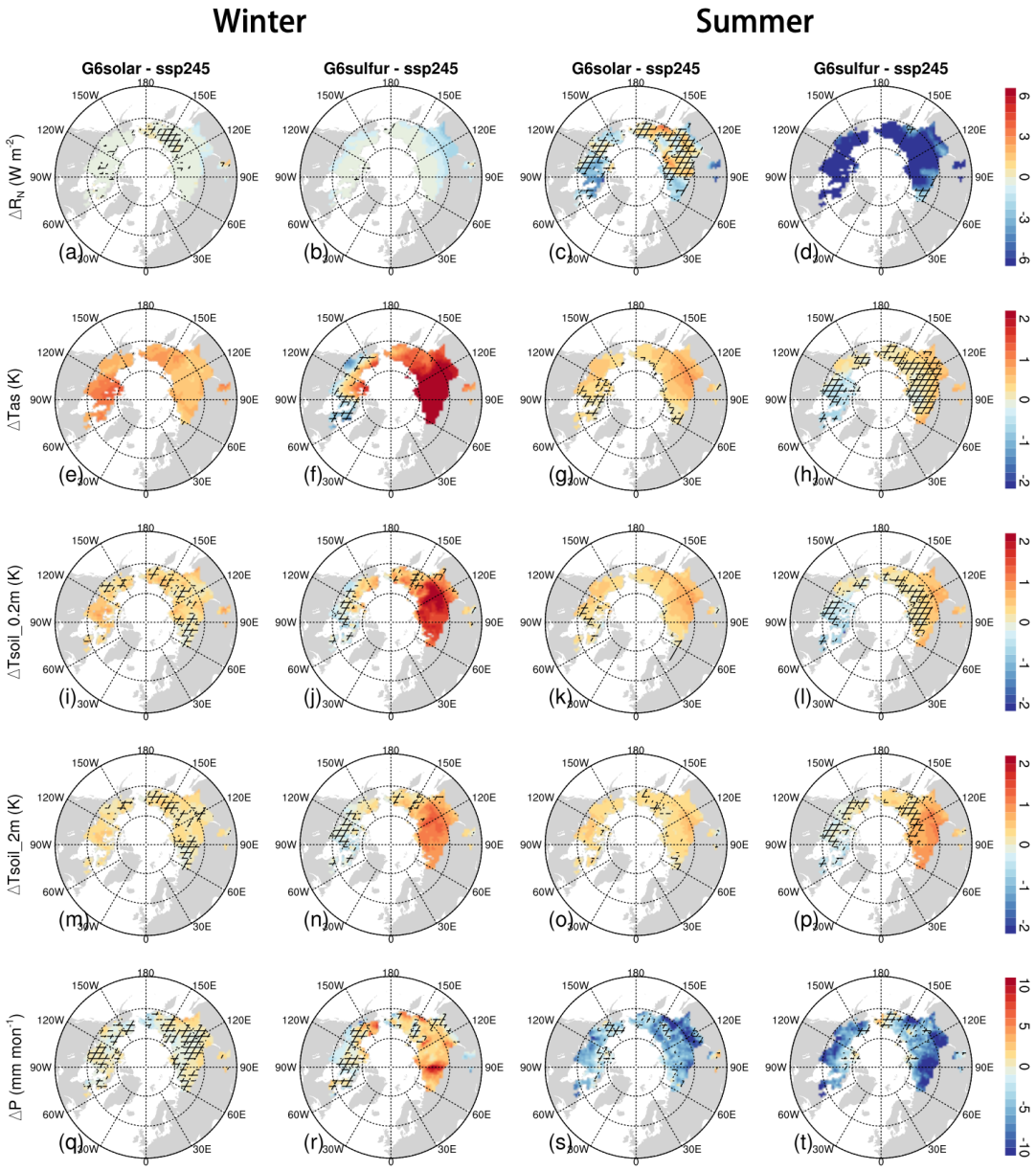

Figure R1. The multi-model ensemble mean changes of surface absorbed shortwave radiation (ΔR_N; a, b, c, d), near-surface air temperature (ΔTas; e, f, g, h), 0.2 m soil temperature (ΔTsoil_0.2m; i, j, k, l), 2 m soil temperature (ΔTsoil_2m; m, n, o, p) and precipitation (ΔP; q, r, s, t) under G6solar, G6sulfur and ssp585 relative to ssp245 during the period 2080-2099 over the baseline $PF_{50\%}$ region. The left two columns show changes in winter (December, January, and February), the right two columns show changes in summer (June, July, and August). The hatched area in each panel indicates where less than 80% of the models (four out of five) agree on the sign of changes in that grid cell.

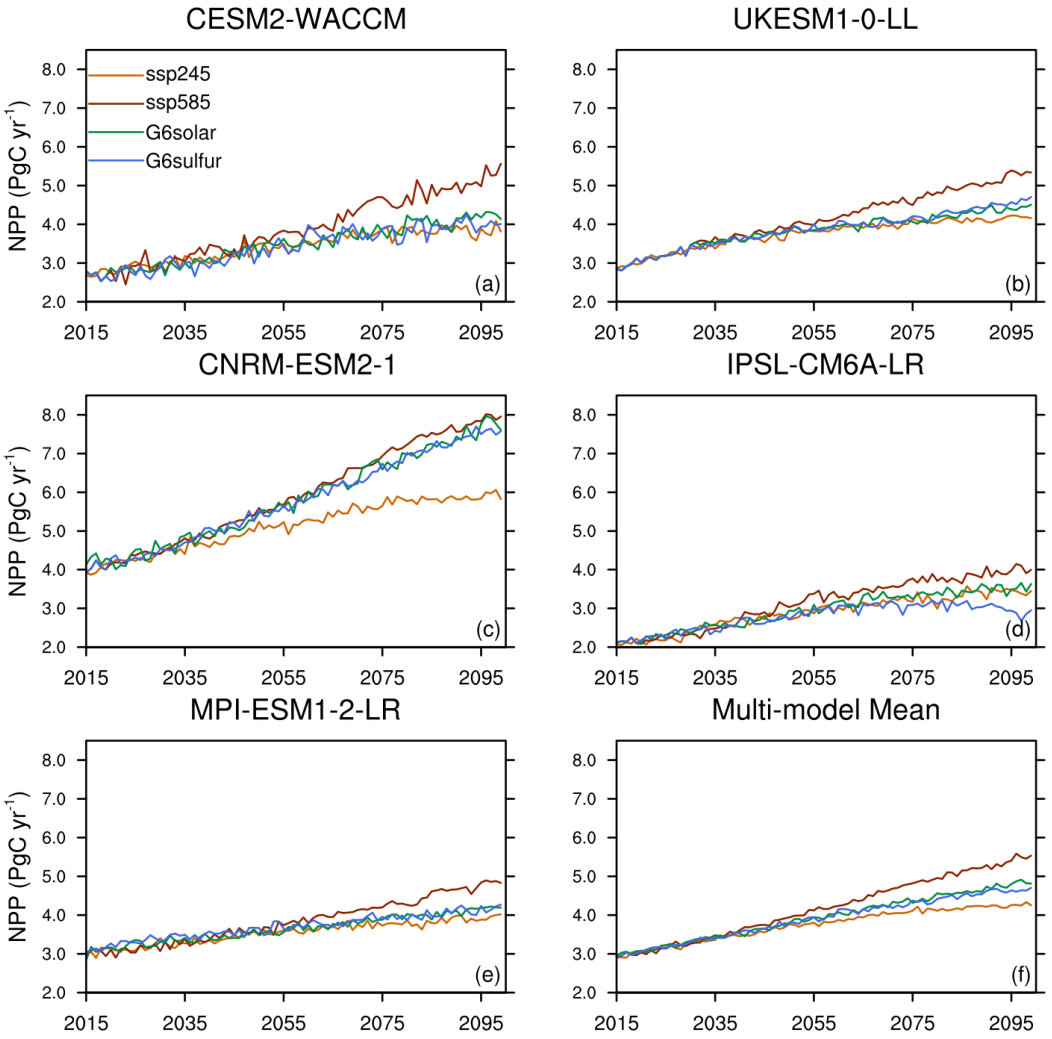

Figure R2. Changes in annual accumulated NPP (Pg C yr^{-1}) for each earth system model during 2015-2099 under ssp245, ssp585, G6solar and G6sulfur. To better show the differences between models, the same range of y-axis is applied for all panels.

2. Also, snow duration and surface litter are important insulators for soil freezing and thawing.

Thanks for your comment. This is clarified and improved in the discussion.

In the baseline period 1995-2014, the average snow duration for grid cells with snow cover fraction ≥ 50% in the $PF_{50\%}$ region from October and March is 5.7, 5.2, 5.7, 5.6 and 4.6 months for CESM2-WACCM, UKESM1-0-LL, CNRM-ESM2-1, IPSL-CM6A-LR and MPI-ESM1-2-LR respectively. Only MPI-ESM1-2-LR shows relatively short snow duration. Longer snow duration tends to exert stronger thermal insulation and show higher soil temperature. On the other hand, the snow insulation simulated by the models depends on the number of snow layers and snow processes represented in its snow scheme as well. To further explore the thermal insulation magnitude of snow and surface litter (or soil organic matter), and their impacts on permafrost area and ALT, the thermal offsets are diagnosed as the difference between soil temperature at 0.2 m depth and near-surface air temperature at 2 m in winter and summer (Figure R3). In combination with the biases in simulated near-surface air temperature, the permafrost derivation from observation can be explained clearly.

The simulated historical permafrost areas, defined by the annual maximum active layer

thicknesses (ALT) ≤3 m, are considerably underestimated in three ESMs (IPSL-CM6A-LR, MPI-ESM1-2-LR and UKESM1-0-LL). The deviation from the observed permafrost status can be ascribed mainly to the biases in the simulated near-surface air temperature and thermal offsets of snow and surface soil layers. UKSEM1-0-LL tends to underestimate summer near-surface air temperature (Figure R3a), but it has a too shallow soil depth of only 3 m (the node depth of bottom layer is less than 3 m) to simulate properly soil temperatures in northern high-latitude. Additionally, its recently added multilayered snow scheme produces a too large snow thermal insulation in winter (Figure R3b), the combined effects lead to a large increase in the mean annual ground temperature (MAGT) and much less permafrost, which has been analyzed in a previous study by Burke et al. (2020). IPSL-CM6A-LR and MPI-ESM1-2-LR show relatively smaller deviation in near-surface air temperature, and they have sufficiently deep soil profiles. But the ground thaws too quickly in the summer, likely because the two models do not consider the latent heat of water-phase change (Burke et al., 2020) and consequently lead to much smaller thermal insulation of top surface layer in summer (Figure R3c). More reasonable representation of northern high-latitude snow and soil processes should be considered in these models in future developments.

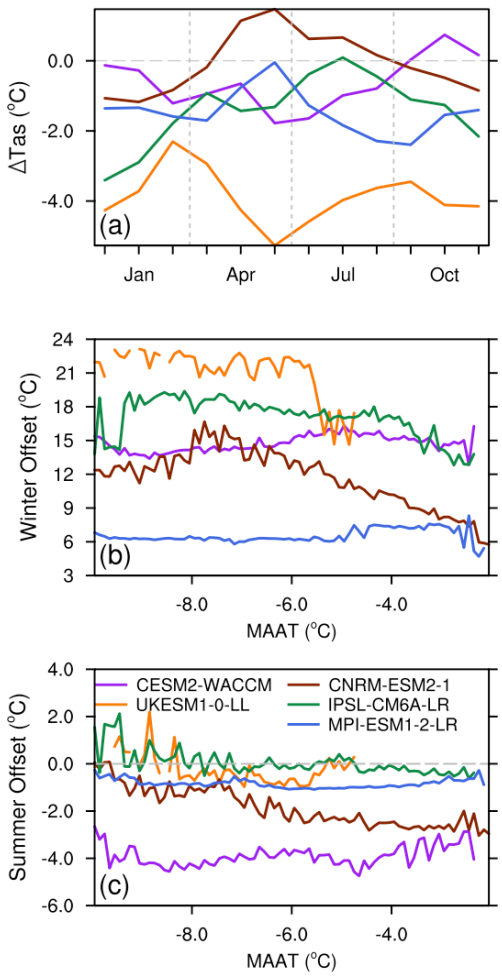

Figure R3. Climatological monthly near-surface air temperature biases and thermal offsets of each ESM. Panel (a) shows the biases in the simulated temperature compared with the observation dataset from Climatic Research Unit gridded Time Series Version 4 (CRU Ts v4, Harris et al., 2020). Panel (b) and (c) show the median values of thermal

offsets vs mean annual air temperature (MAAT) in winter and summer. The thermal offset is calculated as the differences between soil temperature at 0.2 m depth and near-surface air temperature. Only grid cells where the winter mean near-surface air temperatures are between -25 and -15 °C during the baseline period 1995-2014 are shown.

Specific comments

1. Title: to be more specific, like "two solar geoengineering scenarios".

   Thanks. The title is revised to "Northern high-latitude permafrost and terrestrial carbon response to two solar geoengineering scenarios".

2. Line 18, reduce -> reduces.

   Thanks. Line 18 "reduce" is revised to "reduces".

3. Line 18, "including" makes readers confused.

   Agree. We rephrased Line 18 to "Solar geoengineering is a means of mitigating temperature rise and reduces some of the associated climate impacts by increasing the planetary albedo, also the permafrost thaw is expected to be moderated under slower temperature rise. "

4. Line 20-23: I suggest the authors describe more clearly what four scenarios are. Are they two solar geoengineering scenarios based on the settings of ssp245 and ssp585 respectively?

   Thanks. Both G6solar and G6sulfur use ssp585 as the background scenario. They reduce the net anthropogenic radiative forcing from ssp585 to ssp245 by solar irradiance reduction (G6solar) and stratospheric sulfate aerosol injection (G6sulfur). We revised Line 20-23 to "two solar geoengineering scenarios (G6solar and G6sulfur) based on the high emission scenario (ssp585) restore the global temperature from the ssp585 levels to the targeted moderate mitigation scenario (ssp245) levels via solar dimming and stratospheric aerosol injection. "

5. Line 25 to 30: to report results in a quantitative way.

   Thanks for your suggestion. We revised Line 25-30 to "The soil carbon in the northern high-latitude permafrost region increases by 17.7±8.0, 16.4±7.5, 13.6±5.7 and 13.0±8.0 Pg C for G6solar, G6sulfur, ssp245 and ssp585 respectively from the earth system models' simulations. G6solar and G6sulfur accumulate more soil carbon over the northern high-latitude permafrost region due to enhanced CO_2 fertilization effects relative to ssp245 and weakened heterotrophic respiration relative to ssp585. The soil carbon increasing under all four scenarios is mainly due to less decomposition as the multi-model ensemble mean soil carbon storage is greatly underestimated in the northern high-latitude permafrost region.".

6. Line 35: "driven by Arctic amplification", this sentence has a logical mistake. More rapid warming in the north than in the south actually means Arctic amplification.

   Thanks. Line 34-36 is revised to "In the past several decades, the northern high-latitude experienced greater warming than the lower latitudes, recognized as Arctic amplification, and this rapid warming trend is expected to continue in the future (Serreze and Barry, 2011; Biskaborn et al., 2019). "

7. Line 36: renders -> render.

Thanks. Line 36 "renders" is revised to "render".

8. Line 118: Is the G6sulfur run based on the setting of ssp585?

Yes. The G6sulfur run is based on the setting of ssp585. We revised L118 to "G6sulfur is based on ssp585 as well, whereas reduces radiative forcing from ssp585 to ssp245 through stratospheric aerosol injection from 10°S to 10°N along a single longitude band (Kravitz et al., 2015)."

9. Line 122: You need to give some arguments on why the baseline period uses 20 years but the future period uses 10 years.

Thanks. Actually, our analysis for the future period uses the last 20 years of the model simulations, they are average over 2080-2099.

10. Line 163 and 165: How did you linearly interpolate the soil temperature from the surface? The permafrost model should be able to simulate multi-layer soil temperature.

Thank you for your question. Indeed, all the models used in this study have multi-layer soil temperatures, but the vertical discretization of the soil column is uneven amongst models, and soil temperature is only available at the discrete node depths. To derive ALT, we use piecewise linear interpolation to interpolate the monthly soil temperature data to 300 evenly spaced levels (each layer of 0.01m thickness), soil temperatures exceeding 0 ^{o}C is assumed as unfrozen, and the deepest unfrozen depth amongst the year is defined as ALT. For the evenly spaced levels located above the top soil node of model, their temperatures are assumed to be the same as the soil temperature at the top soil node.

11. I suggest the authors add a table or time series for permafrost areal extent, which is complementary to figure 2.

Thank you for your suggestion, we have added the time series for permafrost areal extent in the revised Figure 2.

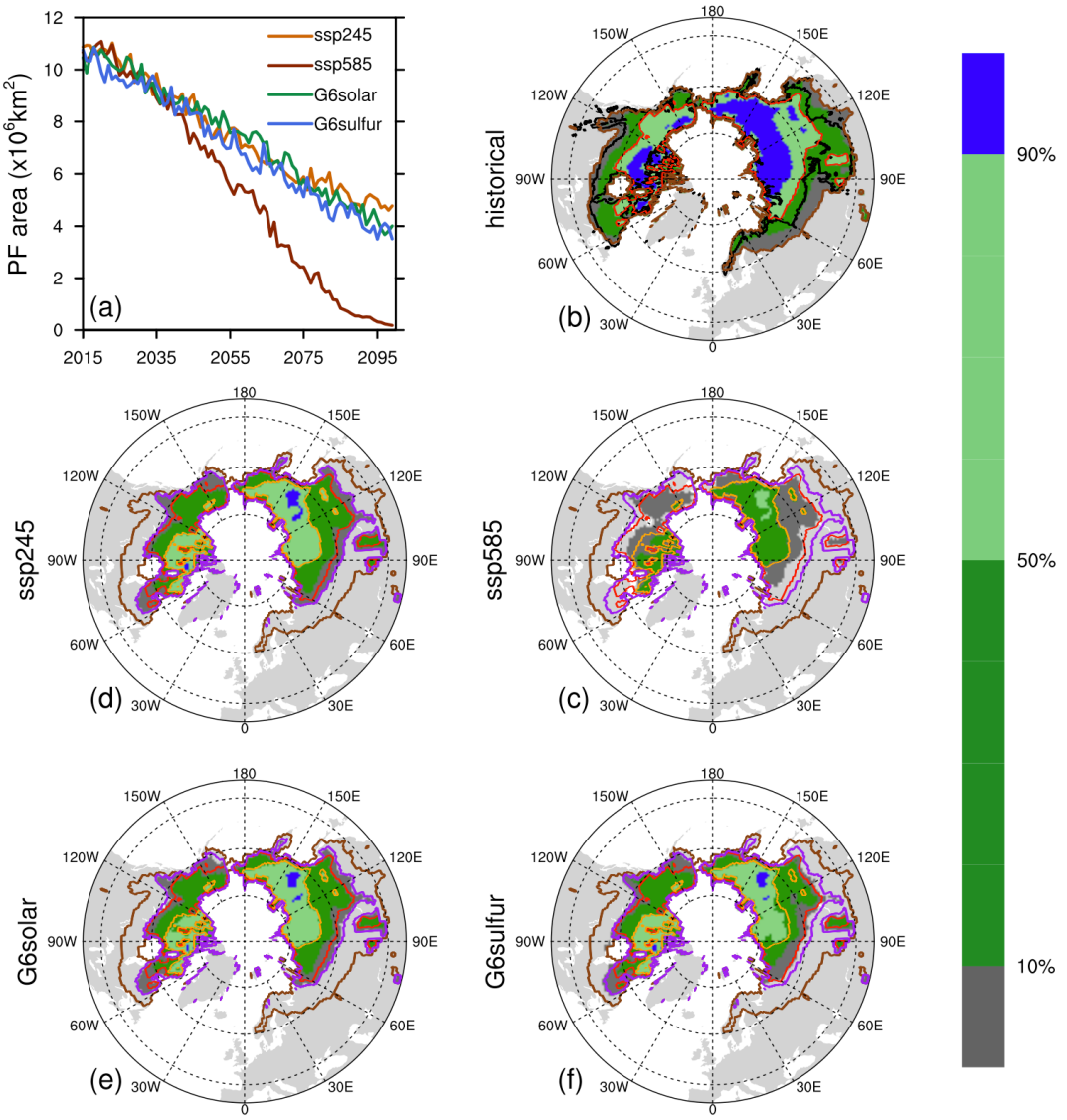

Figure 2. Permafrost area and probability derived according to the observation-based MAAT-permafrost probability relationship (Chadburn et al., 2017). Panel (a) shows multi-model ensemble mean permafrost area change under G6solar, G6sulfur, ssp245 and ssp585. Panels (b-f) show multi-model ensemble mean permafrost probability (shading) and extent (curves) for the last 20 years of each experiment. The black curve in (b) is the extent of the permafrost region defined by IPA permafrost map. The brown and purple curves are the multi-model ensemble mean permafrost extents (permafrost probability ≥ 0.01) for historical and ssp245 simulations, respectively. The red and orange curves are the multi-model ensemble mean permafrost extent where the permafrost probability ≥ 0.5 for historical and ssp245 simulations, respectively.

12. In Figure 3 and Figure 4, I think the authors need to explain why G6solar and G6sulfur have lower radiation and summer temperature but still higher NPP and RH, compared to ssp245.

Thanks for your comments. By direct solar irradiance reduction and radiation reflection by stratospheric aerosol, the downward surface shortwave radiation under G6solar and G6sulfur is lower than ssp245. In contrast, both G6solar and G6sulfur have higher summer temperatures than ssp245, as decreasing insolation and increasing CO_2 modifies the vertical profiles of atmospheric

temperature and atmospheric energy transport. This is the main reason for the residual near-surface warming at high latitudes under solar reduction geoengineering (Henry and Merlis, 2020). The multi-model ensemble mean near-surface air temperature under G6solar and G6sulfur is 0.4±0.1 and 0.1±0.2 ºC higher than ssp245 in summer. Moreover, as G6solar and G6sulfur share the same CO_2 concentrations as ssp585, the stronger CO_2 fertilization effect would facilitate vegetation growth and enhance NPP increasing more than ssp245. Therefore, the higher NPP under G6solar and G6sulfur in summer relative to ssp245 is ascribed to the warmer temperatures and higher CO_2 concentration. Larger RH under G6solar and G6sulfur not only comes from more active soil carbon decomposition under warmer summer temperatures but also from larger amounts of unfrozen soil carbon exposed to microbial activity.

13. Figure 6. In the caption, "G6solar, G6sulfur, and ssp585" need to be reversed in their order.
    Thanks. We revised the order to "ssp585, G6solar and G6sulfur".

14. You should present a figure of ensemble standard deviations from each scenario in the appendix.

    Thanks for your constructive suggestion. We agree on the proper presence of ensemble standard deviations in the manuscripts. The uncertainties of northern high-latitude permafrost and terrestrial responses to future climate in ESM simulations cover many aspects, such as ESMs' response to future climate scenario, the permafrost and terrestrial carbon processes represented in ESMs, and the interactions between all these. To address this issue (and the comments from the other referee), we conducted anomaly-forcing experiments using the latest Community Land Model version 5 (CLM5). The CLM5 is a state-of-the-art land surface model that includes substantial processes associated with permafrost simulation, such as canopy snow processes, cryoturbation, decomposition limitation for frozen soils, vertically resolved soil carbon content (Lawrence et al., 2018). CLM5 can reasonably reproduce historical permafrost extent and soil carbon storage in the northern high-latitude permafrost region (Lawrence et al., 2019).

    CLM5 offers a built-in function supporting the anomaly forcing method by applying precalculated future monthly anomaly signals to user-defined historical sub-daily reference forcing data (Lawrence et al., 2015). In the newly added experiments, monthly anomaly forcing datasets are created for each earth system model's four future climate scenarios (G6solar, G6sulfur, ssp245 and ssp585) against their corresponding historical simulation during the period 2005-2014, including temperature, radiation, precipitation, pressure, wind, and specific humidity. CLM5 reconstructs new sub-daily forcing data by applying these precalculated monthly anomaly forcing on top of the 3-hourly Global Soil Wetness Project forcing dataset (GSWP3, http://hydro.iis.u-tokyo.ac.jp/GSWP3/), which is also used to drive CLM5 for its spin-up and historical simulation from 1850 to 2014.

    Figure R4 shows the multi-model ensemble mean of terrestrial carbon fluxes and carbon stocks changes over the baseline permafrost region and their spreads (plotted as bar charts in each panel). Comparing the spreads of the anomaly forcing CLM5 simulations and the ESMs simulations is helpful to understand the main sources of the uncertainties in the simulated northern high-latitude permafrost and terrestrial carbon response under solar geoengineering scenarios. We will merge this part in the revised manuscript.

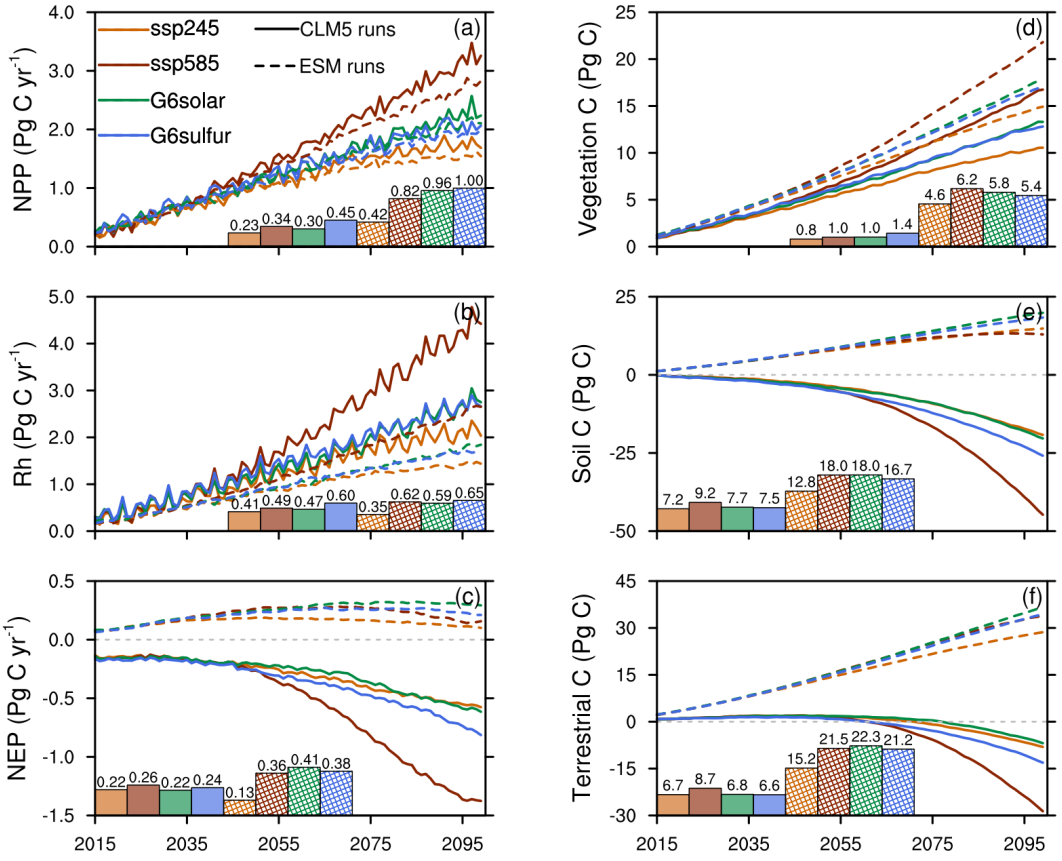

Figure R4. The multi-model ensemble mean of terrestrial carbon fluxes and carbon storage changes over the baseline permafrost region. The left column shows changes in NPP (a), Rh (b) and NEP (c) relative to the baseline period 1995-2014 under ssp245, ssp585, G6solar and G6sulfur. The right column shows changes in vegetation (d), soil (e) and terrestrial (f) carbon storages relative to the baseline period 1995-2014 under ssp245, ssp585, G6solar and G6sulfur. In each panel, bar charts denote one standard derivation from the multi-model ensemble mean averaged over the period 2080-2099, and the number above each bar denotes its magnitude. Dashed lines and hatched bars represent the anomaly forcing CLM5 simulations. Solid lines and solid filled bars represent the ESMs simulations. In panel (c), an 11-year running average is applied on NEP time series to filter its large inter-annual variation.

References:

Arora, V. K., Katavouta, A., Williams, R. G., Jones, C. D., Brovkin, V., Friedlingstein, P., Schwinger, J., Bopp, L., Boucher, O., Cadule, P., Chamberlain, M. A., Christian, J. R., Delire, C., Fisher, R. A., Hajima, T., Ilyina, T., Joetzjer, E., Kawamiya, M., Koven, C. D., Krasting, J. P., Law, R. M., Lawrence, D. M., Lenton, A., Lindsay, K., Pongratz, J., Raddatz, T., Séférian, R., Tachiiri, K., Tjiputra, J. F., Wiltshire, A., Wu, T., and Ziehn, T.: Carbon–concentration and carbon–climate feedbacks in CMIP6 models and their comparison to CMIP5 models, Biogeosciences, 17, 4173-4222, https://doi.org/10.5194/bg-17-4173-2020, 2020.

Biskaborn, B. K., Smith, S. L., Noetzli, J., Matthes, H., Vieira, G., Streletskiy, D. A., Schoeneich, P., Romanovsky, V. E., Lewkowicz, A. G., Abramov, A., Allard, M., Boike, J., Cable, W. L.,

Christiansen, H. H., Delaloye, R., Diekmann, B., Drozdov, D., Etzelmüller, B., Grosse, G., Guglielmin, M., Ingeman-Nielsen, T., Isaksen, K., Ishikawa, M., Johansson, M., Johannsson, H., Joo, A., Kaverin, D., Kholodov, A., Konstantinov, P., Kröger, T., Lambiel, C., Lanckman, J., Luo, D., Malkova, G., Meiklejohn, I., Moskalenko, N., Oliva, M., Phillips, M., Ramos, M., Sannel, A. B. K., Sergeev, D., Seybold, C., Skryabin, P., Vasiliev, A., Wu, Q., Yoshikawa, K., Zheleznyak, M., and Lantuit, H.: Permafrost is warming at a global scale, Nat. Commun., 10, 1-11, https://doi.org/10.1038/s41467-018-08240-4, 2019.

Burke, E. J., Zhang, Y., and Krinner, G.: Evaluating permafrost physics in the Coupled Model Intercomparison Project 6 (CMIP6) models and their sensitivity to climate change, The Cryosphere, 14, 3155-3174, https://doi.org/10.5194/tc-14-3155-2020, 2020.

Burn, C. R., and Zhang, Y.: Sensitivity of active-layer development to winter conditions north of treeline, Mackenzie delta area, western Arctic coast, in: Proceedings of the 6th Canadian Permafrost Conference, The 63rd Canadian Geotechnical Conference, Calgary, Alberta, 12-16 September 2010, http://pubs.aina.ucalgary.ca/cpc/CPC6-1458.pdf, 1458-1465, 2010.

Harris, I., Osborn, T. J., Jones, P., and Lister, D.: Version 4 of the CRU TS monthly high-resolution gridded multivariate climate dataset, Scientific Data, 7, 109, https://doi.org/10.1038/s41597-020-0453-3, 2020.

Henry, M., and Merlis, T. M.: Forcing Dependence of Atmospheric Lapse Rate Changes Dominates Residual Polar Warming in Solar Radiation Management Climate Scenarios, Geophys. Res. Lett., 47, e2020GL087929, https://doi.org/10.1029/2020GL087929, 2020.

Kravitz, B., Robock, A., Forster, P. M., Haywood, J. M., Lawrence, M. G., and Schmidt, H.: An overview of the Geoengineering Model Intercomparison Project (GeoMIP), Journal of Geophysical Research: Atmospheres, 118, 13,103-13,107, https://doi.org/10.1002/2013JD020569, 2013a.

Kravitz, B., Robock, A., Tilmes, S., Boucher, O., English, J. M., Irvine, P. J., Jones, A., Lawrence, M. G., MacCracken, M., Muri, H., Moore, J. C., Niemeier, U., Phipps, S. J., Sillmann, J., Storelvmo, T., Wang, H., and Watanabe, S.: The Geoengineering Model Intercomparison Project Phase 6 (GeoMIP6): simulation design and preliminary results, Geosci. Model Dev., 8, 3379-3392, https://doi.org/10.5194/gmd-8-3379-2015, 2015.

Lawrence, D. M., Koven, C. D., Swenson, S. C., Riley, W. J., and Slater, A. G.: Permafrost thaw and resulting soil moisture changes regulate projected high-latitude CO_2 and CH_4 emissions, Environ. Res. Lett., 10, 094011, https://doi.org/10.1088/1748-9326/10/9/094011, 2015.

Lawrence, D., Fisher, R., Koven, C. D., Oleson, K., Swenson, S., Vertenstein, M. et al., 2018, Technical Description of version 5.0 of the Community Land Model (CLM), http://www.cesm.ucar.edu/models/cesm2/land/CLM50_Tech_Note.pdf

Lawrence, D. M., Fisher, R. A., Koven, C. D., Oleson, K. W., Swenson, S. C., Bonan, G., Collier, N.,

Ghimire, B., van Kampenhout, L., Kennedy, D., Kluzek, E., Lawrence, P. J., Li, F., Li, H., Lombardozzi, D., Riley, W. J., Sacks, W. J., Shi, M., Vertenstein, M., Wieder, W. R., Xu, C., Ali, A. A., Badger, A. M., Bisht, G., van den Broeke, M., Brunke, M. A., Burns, S. P., Buzan, J., Clark, M., Craig, A., Dahlin, K., Drewniak, B., Fisher, J. B., Flanner, M., Fox, A. M., Gentine, P., Hoffman, F., Keppel Aleks, G., Knox, R., Kumar, S., Lenaerts, J., Leung, L. R., Lipscomb, W. H., Lu, Y., Pandey, A., Pelletier, J. D., Perket, J., Randerson, J. T., Ricciuto, D. M., Sanderson, B. M., Slater, A., Subin, Z. M., Tang, J., Thomas, R. Q., Val Martin, M., and Zeng, X.: The Community Land Model Version 5: Description of New Features, Benchmarking, and Impact of Forcing Uncertainty, J. Adv. Model. Earth Sy., 11, 4245-4287, https://doi.org/10.1029/2018MS001583, 2019.

Muri, H., Tjiputra, J., Otterå, O. H., Adakudlu, M., Lauvset, S. K., Grini, A., Schulz, M., Niemeier, U., and Kristjánsson, J. E.: Climate Response to Aerosol Geoengineering: A Multimethod Comparison, J. Climate, 31, 6319-6340, https://doi.org/10.1175/JCLI-D-17-0620.1, 2018.

Russotto, R. D., and Ackerman, T. P.: Energy transport, polar amplification, and ITCZ shifts in the GeoMIP G1 ensemble, Atmos. Chem. Phys., 18, 2287-2305, https://doi.org/10.5194/acp-18-2287-2018, 2018.

Serreze, M. C., and Barry, R. G.: Processes and impacts of Arctic amplification: A research synthesis, Global Planet. Change, 77, 85-96, https://doi.org/10.1016/j.gloplacha.2011.03.004, 2011.

Visioni, D., MacMartin, D. G., Kravitz, B., Boucher, O., Jones, A., Lurton, T., Martine, M., Mills, M. J., Nabat, P., Niemeier, U., S Ef Erian, R., and Tilmes, S.: Identifying the sources of uncertainty in climate model simulations of solar radiation modification with the G6sulfur and G6solar Geoengineering Model Intercomparison Project (GeoMIP) simulations, Atmos. Chem. Phys., 21, 10039-10063, https://doi.org/10.5194/acp-21-10039-2021, 2021.

Yu, X., Moore, J. C., Cui, X., Rinke, A., Ji, D., Kravitz, B., and Yoon, J.: Impacts, effectiveness and regional inequalities of the GeoMIP G1 to G4 solar radiation management scenarios, Global Planet. Change, 129, 10-22, https://doi.org/10.1016/j.gloplacha.2015.02.010, 2015.